

***Final Draft***  
**of the original manuscript:**

Victoria-Hernandez, J.; Yi, S.; Letzig, D.; Hernandez-Silva, D.; Bohlen, J.:  
**Microstructure and texture development in hydrostatically  
extruded MgAlZn alloys during tensile testing at intermediate  
temperatures**

In: Acta Materialia (2013) Elsevier

DOI: [10.1016/j.actamat.2012.12.039](https://doi.org/10.1016/j.actamat.2012.12.039)

# Microstructure and texture development in hydrostatically extruded Mg-Al-Zn alloys during tensile testing at intermediate temperatures

J. Victoria-Hernandez<sup>1</sup>, S. Yi<sup>1</sup>, D. Letzig<sup>1</sup>, D. Hernandez-Silva<sup>2</sup>, and J. Bohlen<sup>1</sup>

<sup>1</sup>Magnesium Innovation Centre MagIC, Helmholtz-Zentrum Geesthacht, Max-Planck-Strasse 1, D-21502 Geesthacht, Germany

<sup>2</sup>Department of Metallurgical Engineering, Instituto Politécnico Nacional-ESIQIE, Apdo. Postal 118-392, 07738 Mexico City, Mexico

## Abstract

Tensile testing of hydrostatically extruded round bars of AZ31 and AZ61 has been performed to analyse the flow behaviour as well as the microstructure and texture development as a function of temperature (175–225 °C) and strain rate (0.0001–0.01 s<sup>-1</sup>). The post-testing microstructure is a result of dynamic recrystallisation with varying significance of different texture components. In some cases the resulting textures are found to be similar to those textures that typically develop during extrusion of rare earth containing magnesium alloys. Dynamic recrystallisation (DRX) and grain boundary sliding (GBS) are considered as the mechanisms that generate the changes in texture. Precipitates can exert a grain boundary pinning effect limiting grain growth. These different mechanisms contribute differently to the texture development if the testing parameters were changed.

Key words: Magnesium alloys, Texture, Dynamic recrystallisation, Grain boundary sliding, Particle pinning.

## 1. Introduction

Typical wrought magnesium alloys tend to form strong textures during forming processes. In magnesium extrusions, a prismatic  $\langle 10.0 \rangle$ - $\langle 11.0 \rangle$  double fibre texture is often found, which orients the basal planes parallel to the extrusion direction [1,2]. It is known that such textures restrict the availability of potentially active basal slip during deformation especially at room temperature and are therefore unfavourable for

ductility. Primary slip in Mg with its hexagonal close packed lattice structure takes place on the basal plane (0001) and secondary slip on the prismatic planes ( $10\bar{1}0$ ), both in the  $\langle 11\bar{2}0 \rangle$  direction. Furthermore, twinning on the  $\{10\bar{1}2\}$  and  $\{10\bar{1}1\}$  planes can contribute to strain accommodation. If extension along the c-axis of the lattice is required, extension twinning on the  $\{10\bar{1}2\}$  planes can easily be activated. This leads to distinct yield and flow asymmetries if the behaviour in tension and compression is compared. On the other hand, if compression along the c-axis is required,  $\{10\bar{1}1\}$  contraction twinning might be activated [3,4]. However, it is suggested that their contribution to the total deformation is rather small [5]. Alternatively, pyramidal  $\langle c+a \rangle$  slip can accommodate compressive strain along the c-axis. This slip mode can also be activated but only at elevated temperatures or in the presence of certain alloying additions. Increased activity of pyramidal  $\langle c+a \rangle$  slip has been reported in a Mg-3 wt. % Y alloy deformed at room temperature [6]. Activation of this additional deformation mode leads to more homogeneous deformation, a reduction in the strength of the basal texture and higher ductility compared with pure Mg. However, if deformation is mainly accommodated by basal slip or extension twinning, strong textures with preferential orientation of the basal planes parallel to the extrusion direction are likely to develop as a result of re-orientation during processing.

During thermomechanical treatments, dynamic recrystallisation (DRX) has a strong effect on the mechanical behaviour and on the development of texture [7]. DRX leads to the formation of new grains during the deformation process. Two main mechanisms have been discussed in this context: One of these is discontinuous dynamic recrystallisation (dDRX); the other is rotational dynamic recrystallisation (rDRX). In the former, new grains are mainly formed at grain boundaries and form a

mantle around them by grain boundary bulging due to strain-induced boundary migration [8]. The dDRXed grains are therefore expected to be relatively strain-free. On the other hand, rDRX involves a progressive rotation of subgrains adjacent to pre-existing grain boundaries as the material is strained. A mantle of recrystallised grains along grain boundaries is also formed, but with the old grains developing a gradient of misorientation from the centre to the edge. Both dDRX and rDRX have been used to explain experimental observations in Mg alloys [9, 10]. The influence of these different recrystallisation mechanisms on texture development has been considered as a possible explanation for the weaker textures that can develop during rolling or extrusion [11], especially in the context of magnesium alloys that contain a certain amount of rare earth (RE) alloying elements. These weaker textures no longer exhibit a distinct basal fibre component, but tend to show off-basal peaks [12, 13] and a broader orientation distribution of the basal planes towards the transverse direction (TD) rather than towards the rolling direction (RD). In the case of round bar extrusions, textures have also been found which exhibit a weak  $\langle 11.1 \rangle$  texture component at the expense of the conventional  $\langle 10.0 \rangle$ - $\langle 11.0 \rangle$  fibre texture [14, 15, 16]. The result is that the basal planes are no longer strongly aligned in the extrusion direction but show a preferential tilt of 20–40° away from the extrusion direction. This texture also leads to improved ductility of the processed material.

Recent studies have shown that the origin of such textures is most likely to be a consequence of the influence of RE elements on the recrystallisation behaviour within shear bands produced during thermomechanical processing [7, 14, 15, 17].

Ball and Pragnell [18] hypothesized that texture weakening during deformation processing could be a result of particle stimulated nucleation (PSN) of recrystallisation during DRX. PSN originates at pre-existing subgrains within the

deformation zone around a particle and occurs when the accumulation of misorientation by a rapid sub-boundary migration generates the necessary high angle grain boundaries (HAGB) that can form a new grain nucleus which has the possibility to grow and form a new recrystallised grain. The orientation of the recrystallisation nuclei produced by PSN will be different from those produced by other recrystallisation mechanisms [19].

Furthermore, it has been shown that rare earth elements tend to restrict grain boundary migration, an effect which might change the significance of different fractions of the microstructure and their influence on texture.

Recently, very high ductility and textures which showed similarities to the ones of extruded Mg-RE alloys were found in a conventional AZ61 alloy tested in tension at temperatures as low as 175 °C [20]. Based on these earlier results, this paper will deal with an analysis of the development of texture during tensile deformation of the alloys AZ31 and AZ61 using electron backscatter diffraction (EBSD). The aim of this work is to clarify the role of recrystallisation mechanisms in the formation of textures that, up to now, have not yet been reported in Mg-Al-Zn alloys. Since the stress conditions during conventional tensile testing and round bar extrusion are quite similar, similarities between the two treatments can be described.

## **2. Experimental procedures**

In this study, the alloys AZ31 (2.8 wt.% Al-0.9 wt.% Zn-0.2 wt.% Mn) and AZ61 (6.3 wt.% Al-0.9 wt.% Zn-0.2 wt.% Mn) processed by hydrostatic extrusion were used. Cone-shaped billets of these alloys were cast and then heated to 150 °C. Extrusion was carried out to produce round bars with diameters of 12 mm which corresponds to an extrusion ratio of 1:28. The die exit speed of the profiles (extrusion

rate) was 8 m/min. After exiting the die, the profiles were quenched to room temperature using a water spray. Details on the processing methods and related experiments can be found in reference [21].

Samples with a diameter of 4 mm and a gauge length of 24 mm were machined with their longitudinal axis parallel to the extrusion direction for tensile testing with a universal testing machine equipped with a fan-driven furnace (Zwick Z050). Tension tests up to fracture were carried out at temperatures of 175, 200 and 225 °C at strain rates of  $10^{-2}$ ,  $10^{-3}$  and  $10^{-4}$  s<sup>-1</sup>. After fracture, the samples were immediately quenched to room temperature in a water bath in order to retain the microstructure and texture.

Electron backscatter diffraction (EBSD) was carried out using a field emission gun scanning electron microscope (Zeiss™, Ultra 55) equipped with an EDAX/TSL EBSD system with a Hikari detector. Longitudinal sections of the tensile samples were ground (sandpaper grit: 800-1000-1200 and 4000) and mechanically polished with 1 µm alumina powder. Electro-chemical polishing was then carried out using a Struers™ AC2 solution at 16 V for 80 s at -15 °C. EBSD measurements were performed at an accelerating voltage of 15 kV and a step size of 0.2 µm. In the case of fractured samples the measurements were carried out near the fracture tip. Local orientation maps were used to reveal the microstructure and texture of the samples.

In addition, energy-dispersive X-ray spectroscopy (EDS) was performed on the same samples in order to reveal the type and chemical composition of the particles formed during deformation.

### **3. Results**

Fig. 1 shows EBSD orientation maps and the corresponding inverse pole figures (IPF) in the extrusion direction of the as-extruded AZ31 and AZ61 bars. Due to the

symmetry of the round bar extrusion, the IPF contains all relevant information to describe the texture, and therefore, this representation will be used.

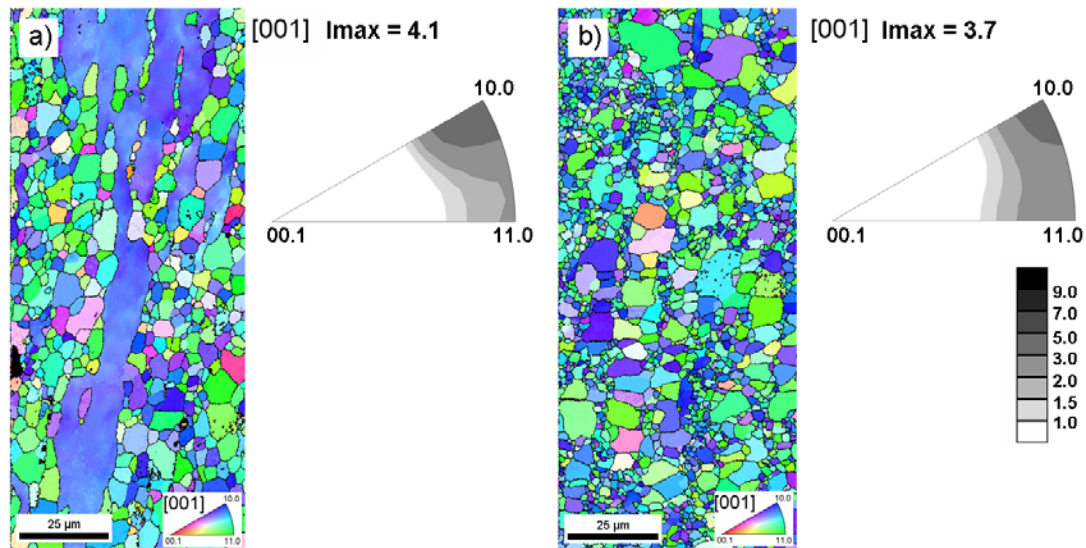


Fig. 1: EBSD orientation maps and texture distributions in the as-extruded condition: a) AZ31 and b) AZ61.

The AZ31 bar exhibits a microstructure with a rather broad grain size distribution and some large elongated grains parallel to the extrusion direction, Fig. 1a. These elongated grains are surrounded by small equiaxed recrystallised grains. The average grain size of the equiaxed grains is  $5 \mu\text{m}$ . This alloy exhibits a typical  $\langle 10.0 \rangle$  fibre texture with the majority of grains therefore having their basal planes oriented parallel to the extrusion direction. Furthermore, higher intensities are found preferentially along the arc between the  $\langle 10.0 \rangle$  and  $\langle 11.0 \rangle$  poles. In the case of AZ61, Fig. 1b, the microstructure does not exhibit the above mentioned large long grains, but also has a broad grain size distribution with an average grain size of  $5 \mu\text{m}$ . The texture of this alloy is basically comparable to that of AZ31. However, the intensity of the  $\langle 10.0 \rangle$  pole is slightly weaker.

Examples of the true stress-true strain curves for both alloys tested in tension at 175, 200 and 225 °C and a strain rate of  $10^{-3} \text{s}^{-1}$  are shown in Fig. 2.

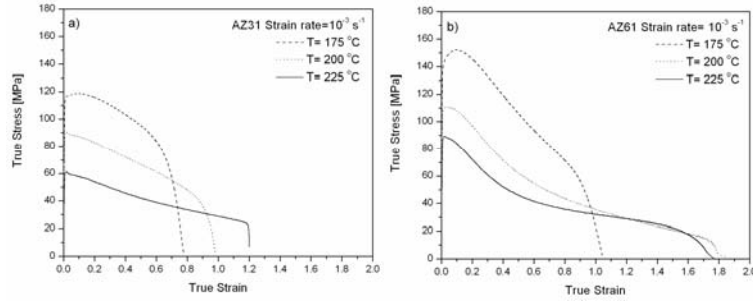


Fig. 2: Stress-strain curves at 175, 200 and 225 °C and  $10^{-3} \text{ s}^{-1}$ : a) AZ31 and b) AZ61.

In general, the flow stress decreases with increasing temperature. Both alloys are very ductile even at the lowest test temperature of 175 °C. The AZ61 alloy exhibits larger elongations to failure compared to AZ31. At all testing temperatures the curves reveal initial work hardening until a peak stress is attained, which is followed by rapid work softening. This behaviour is typical for materials undergoing DRX [9, 22, 23]. The subsequent decrease in the flow stress is observed for all strain rates used. This decrease is less pronounced in AZ31, Fig. 2a, whereas in AZ61 it is continuous until the end of the tests where low stresses are recorded without abrupt failure, Fig. 2b.

Samples tested to fracture were used to study the microstructural development as a function of the applied testing parameters. It is recognized that the dependency of the flow stress on temperature  $T$  and strain rate  $\dot{\epsilon}$  can be described by a single factor, the temperature compensated strain rate  $Z$  which is a parameter named after Zener and Hollomon [24],

$$Z = \dot{\epsilon} \cdot \exp\left(\frac{Q}{RT}\right) \quad (1)$$

where  $R$  is the gas constant and  $Q$  is the effective activation energy for deformation. The dependency of the flow stress of an experiment can then be reduced to this parameter. A general description which is commonly used [22] is a hyperbolic law

$$Z = \dot{\varepsilon} \cdot \exp\left(\frac{Q}{RT}\right) = A \cdot (\sinh(\alpha\sigma))^n \quad (2)$$

where  $A$ ,  $\alpha$  and  $n$  are material constants that are considered to be independent of  $T$ , strain rate and stress. There are several procedures used to derive the material constants, e.g. [23, 25]. In this work, the peak stress is taken from the flow curves as the only significant parameter for evaluation with Eqn. 2. The results are displayed in Table 1. The activation energy  $Q$  is higher for AZ61 than for AZ31 which is consistent with the larger amount of precipitates as well as the higher aluminium content in AZ61.

Table 1: Material constants of hydrostatically extruded AZ31 and AZ61 bars according to Equation 2

Alloy	$Q$ [kJ/mol]	$\alpha$ [MPa <sup>-1</sup> ]	$n$	$\ln(A)$
AZ31	119 (13)	0.013 (0.003)	3.3 (0.1)	22.44 (0.08)
AZ61	141 (3)	0.009 (0.002)	4.7 (0.1)	28.05 (0.06)

Fig. 3 shows the peak stresses and fracture strains as a function of  $Z$ . A continuous increase of the peak stress with increasing  $Z$  is observed for both alloys. Furthermore, a continuous decrease of the fracture strain with increasing  $Z$  is found for AZ31 (Fig. 3a). In AZ61 an increase of the peak stress is also found with increasing  $Z$ , whereas the fracture strain exhibits more complex behaviour (Fig. 3b). With increasing  $Z$ , the fracture strain first increases to a peak value and then decreases.

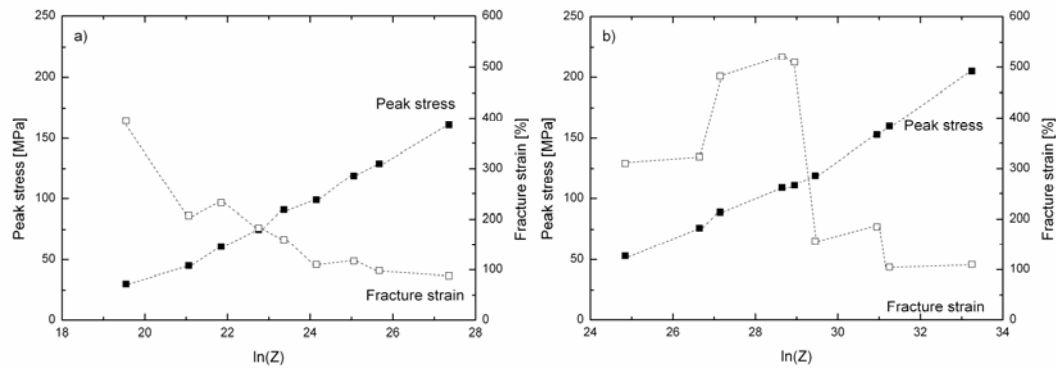


Fig. 3: Peak stress and fracture strain as a function of  $Z$ . a) AZ31 and b) AZ61 (Dashed lines are shown to guide the eye).

Analysis of the microstructures after fracture was carried out using EBSD orientation mapping. Typical examples of this series of measurements are shown in Fig. 4a-c for AZ31 and Fig. 4d-f for AZ61. After testing AZ31 at 175 °C and  $10^{-2} \text{ s}^{-1}$ , a bimodal microstructure is found with elongated grains surrounded by small equiaxed grains, (Fig. 4a). This microstructure is qualitatively similar to that in the as-extruded condition and is understood to be a partially recrystallised microstructure having unrecrystallised elongated grains and newly formed recrystallised grains. At the lower strain rate of  $10^{-4} \text{ s}^{-1}$ , such elongated grains are not observed and a fine-grained microstructure is found, (Fig. 4b). After testing at 200 °C with the low strain rate, a coarser-grained microstructure is observed, (Fig. 4c). Similar features can also be seen in Fig. 4d-f for the AZ61 samples. For this alloy, it is noteworthy that larger fractions of the microstructure are identified as precipitates of  $\text{Mg}_{17}\text{Al}_{12}$  which leave unidentified fractions of the microstructure if only indexed for magnesium.

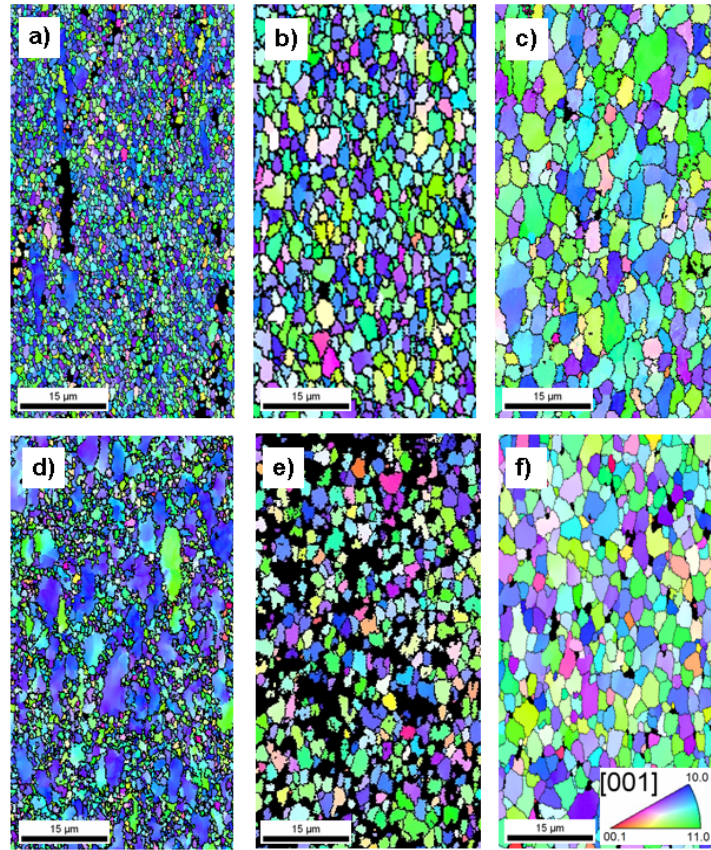


Fig. 4: Orientation maps of AZ31 samples tested at a)  $175\text{ }^{\circ}\text{C}/10^{-2}\text{ s}^{-1}$ , b)  $175\text{ }^{\circ}\text{C}/10^{-4}\text{ s}^{-1}$  and c)  $200\text{ }^{\circ}\text{C}/10^{-4}\text{ s}^{-1}$  and AZ61 samples with the same testing parameters d), e) and f), respectively.

Fig. 5 summarises the average grain sizes after tensile deformation as a function of  $Z$  for both alloys. Two different measures of grain size are used in this analysis. One is the average grain size of the whole microstructure, typically named the average grain size. The other is the average grain size of the recrystallised fraction of the microstructure, named the average recrystallised grain size. The fraction of the microstructure which provides the latter value is separated by using the assumption that recrystallised grains should have a low internal grain orientation spread (GOS), see e.g. [8, 16]. Thus, a limiting value of  $\text{GOS} < 1\text{ }^{\circ}$  is used to define recrystallised grains. The resulting grain size data are plotted in Fig. 5.

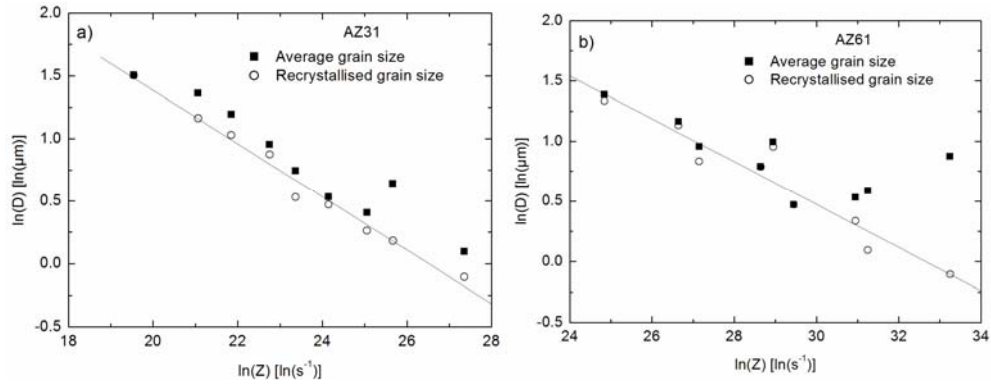


Fig. 5: Average grain size (filled symbols) and average recrystallised grain size (open symbols) as measured in quenched samples after tensile testing as a function of  $Z$  for a) AZ31 and b) AZ61

The average recrystallised grain size in AZ31 decreases continuously with increasing  $Z$ . The average grain size of the whole microstructure also shows the same tendency, but the grain sizes are slightly larger and especially at higher  $Z$ , a larger scatter in the data is found. The same scatter is found for AZ61 at high  $Z$  with even higher significance. This is explained by the incomplete recrystallisation observed under these conditions ( $175, 200 \text{ }^\circ\text{C}/10^{-2} \text{ s}^{-1}$ ) where some coarse unrecrystallised grains are found between the newly recrystallised grains. It is noteworthy that these samples are also those with the lowest fracture strains, which is likely to limit the fraction of recrystallised microstructure. If only the recrystallised grain size data are considered, the influence of temperature and strain rate is the same as for AZ31.

The EBSD measurements on samples of both alloys after fracture were also used to recalculate inverse pole figures in the tensile loading direction as shown in Fig. 6. The pole figures are ordered according to decreasing  $Z$ . Fig. 6a shows the results for AZ31. The maximum intensity in the inverse pole figures first slightly decreases with decreasing  $Z$  but then increases again. This is understood as a result of the changing significance of a number of texture components. At high  $Z$ , the pole figures exhibit higher intensities along the arc between the  $\langle 10.0 \rangle$  and  $\langle 11.0 \rangle$  poles and a higher intensity at the  $\langle 10.0 \rangle$  pole. With decreasing  $Z$ , the  $\langle 11.0 \rangle$  pole component becomes

more significant and results in the final increase of the maximum pole figure intensity. This is often experienced in magnesium extrusions if the material has the possibility to completely recrystallise [8]. Furthermore, after some tests, especially at 200 °C and  $10^{-2} \text{ s}^{-1}$  as well as 175 °C and  $10^{-3} \text{ s}^{-1}$ , the  $\langle 11.0 \rangle$  component is not significant and a texture results which exhibits orientations around the  $\langle 11.1 \rangle$  pole (see the arrows in Fig. 6a). A pronounced intensity at this pole has hitherto only been found in magnesium extrusions containing rare earth elements [7, 16, 17]. Fig. 6b shows a very similar result for AZ61 which is even more distinct. With decreasing Z, the  $\langle 10.0 \rangle$  pole intensity tends to decrease. In some cases, a more or less equal intensity distribution develops along the arc between the  $\langle 10.0 \rangle$  and the  $\langle 11.0 \rangle$  poles, especially at the lowest Z. In other cases, the intensity distribution is generally low and only distinct along an arc between the  $\langle 10.0 \rangle$  and  $\langle 11.1 \rangle$  poles. In this alloy, the texture intensity around the  $\langle 11.1 \rangle$  pole is observed for a wider range of testing conditions compared to the AZ31 alloy. In addition, higher intensity appears around the  $\langle 20.1 \rangle$  pole after testing at 200 °C/ $10^{-4} \text{ s}^{-1}$  (see the arrows in Fig. 6b). It is worth noting that in both alloys, there is a higher intensity around the  $\langle 11.1 \rangle$  pole that is more visible after testing at 175 °C and  $10^{-4} \text{ s}^{-1}$ . Under these testing conditions, the maximum intensity is around this pole and the intensities at the  $\langle 10.0 \rangle$  and  $\langle 11.0 \rangle$  poles are significantly reduced.

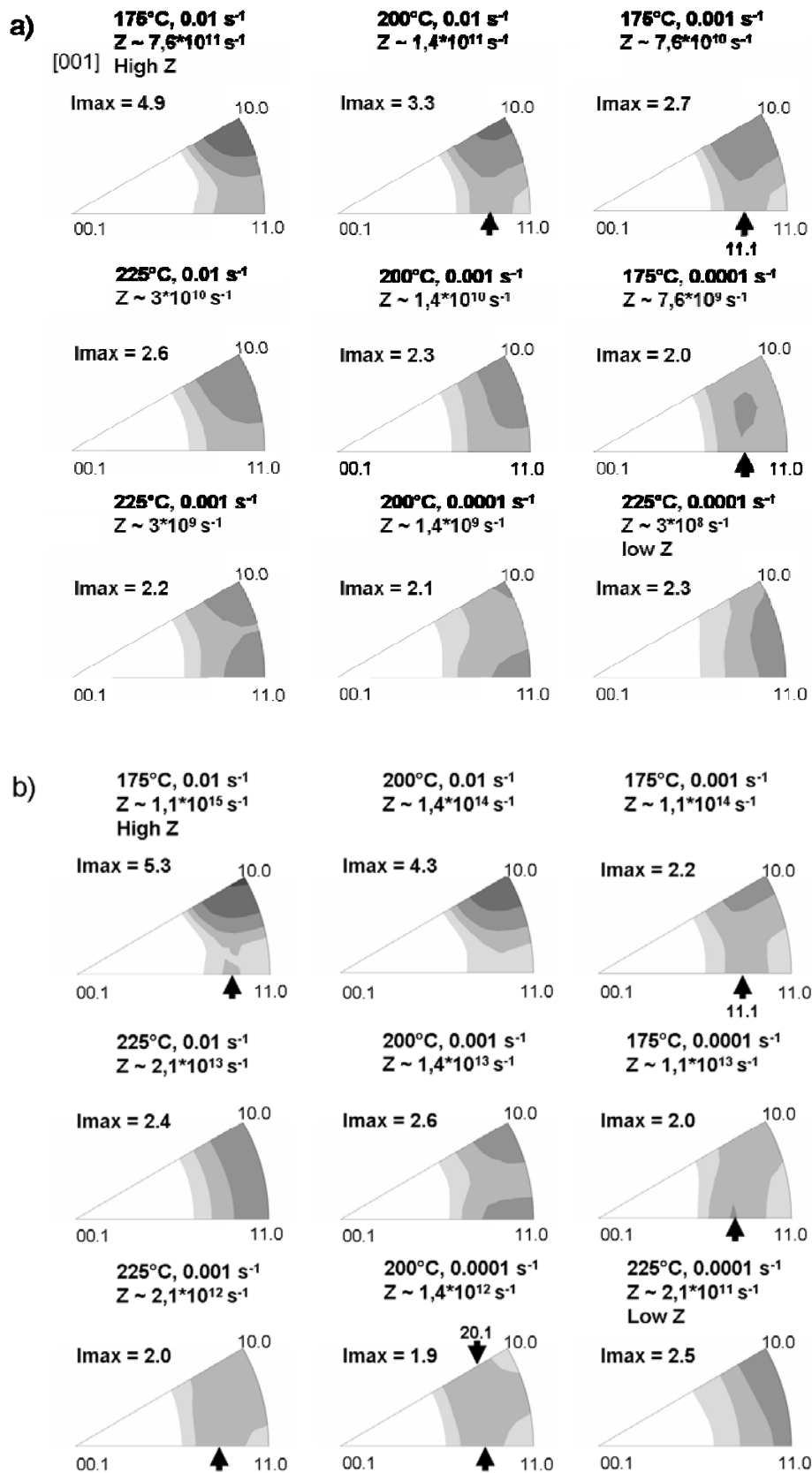


Fig. 6: Inverse pole figures of AZ31 (a) and AZ61 (b) tested at temperatures from 175 to 225 °C and strain rates from 10<sup>-2</sup> to 10<sup>-4</sup> s<sup>-1</sup> as a function of Z.

It is also seen in Figs. 6a and 6b that the intensities around the  $\langle 11.1 \rangle$  pole are not necessarily the result of a distinct texture component because intensities at this pole are quite comparable for all presented tests. It especially becomes visible due to the relatively lower number of grains with  $\langle 11.0 \rangle$  orientation.

In order to reveal the significance of this and other texture poles, the intensities measured at the  $\langle 10.0 \rangle$ ,  $\langle 11.0 \rangle$ , and  $\langle 11.1 \rangle$  poles of the IPF are plotted as a function of  $Z$  in Fig. 7. A continuous decrease of the  $\langle 10.0 \rangle$  pole intensity with decreasing  $Z$  is observed for both alloys, whereas the  $\langle 11.0 \rangle$  and the  $\langle 11.1 \rangle$  pole intensities remain more or less constant for all testing conditions (see Fig. 7a for AZ31 and Fig. 7b for AZ61).

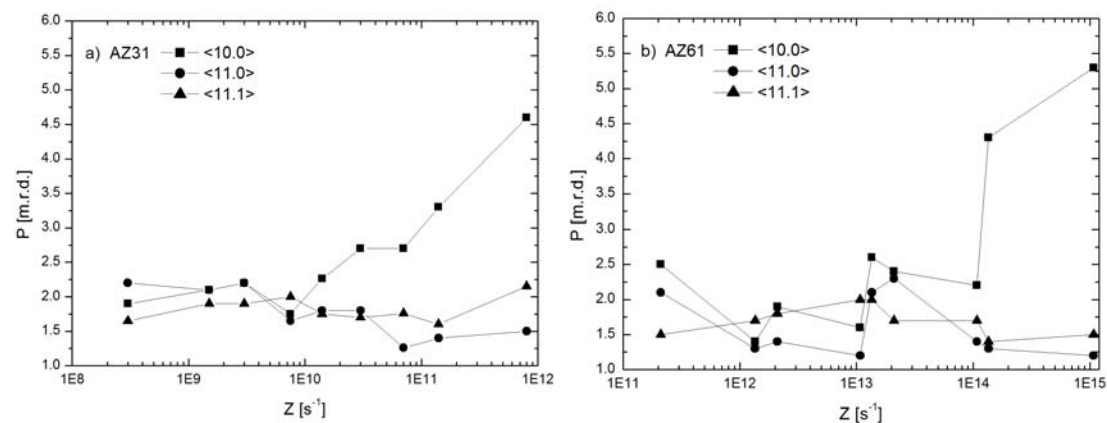


Fig. 7: Variation of the  $\langle 10.0 \rangle$ ,  $\langle 11.0 \rangle$ , and  $\langle 11.1 \rangle$  pole intensities as a function of  $Z$  for a) AZ31 and b) AZ61.

## 4. Discussion

### 4.1 Microstructural development

The microstructure generated during tensile testing is mainly a result of dynamic recrystallisation as confirmed by the results shown in Figs. 4 and 5. Although it is hard to distinguish different fractions of the microstructure, i.e. deformed grains remaining from the extruded microstructure and newly formed grains resulting from dynamic recrystallisation, the assumption of a low internal GOS within the

recrystallised grains appears appropriate. This concept has been used in earlier work to separate the recrystallised fraction of the microstructure in EBSD orientation maps [8, 16]. The results presented in Fig. 5 are generally consistent with the expectation of a decrease in the recrystallised grain size with increasing  $Z$ , confirming an expected influence of the testing parameters on the microstructure development due to DRX. Only at high  $Z$  (and therefore high strain rate, i.e.  $10^{-2} \text{ s}^{-1}$ ) are some larger grains with higher GOS values found. These dominate the microstructure and lead to an increase in the average grain size, whereas the recrystallised grain size is still small. It is worth emphasising that the presence of such unrecrystallised grains is limited to those samples with the lowest fracture strains, for which a smaller fraction of dynamically recrystallised microstructure is expected. On the other hand, samples with high fracture strains have a large fraction of grains with low GOS and can therefore be considered as almost fully recrystallised. The lower is  $Z$ , the larger the corresponding grain size.

#### *4.2 Texture development*

Differences in the texture after testing can be correlated with the degree of recrystallisation of the material. Samples with low fracture strains and therefore only partially recrystallised microstructures, i.e. the experiments at larger  $Z$ , exhibit a strong  $\langle 10.0 \rangle$  fibre component which is related to the unrecrystallised remains of the original microstructure. In the case of the AZ61 alloy, samples having a significantly larger fracture strain show unusual textures with a higher intensity around the  $\langle 11.1 \rangle$  pole rather than the typical  $\langle 11.0 \rangle$  component. However, comparable textures develop in samples of the AZ31 alloy at considerably smaller fracture strains. Thus, the appearance of this texture is not only a result of high fracture strains achieved in the

respective samples which is directly correlated to an increase of the fraction of the recrystallised microstructure. Therefore, an analysis of the influence of the unrecrystallised and the recrystallised fraction of the microstructure on the texture development is required.

#### *4.3 The unrecrystallised fraction of the microstructure*

Similar to the considerations about the recrystallised fraction of the microstructure, a larger GOS can serve as a separating constraint for the unrecrystallised fraction of the microstructure. The inverse pole figures of the fraction of the microstructure with a  $GOS > 2^\circ$  are illustrated in Fig. 8. In this analysis the results are presented in terms of both temperature and strain rate in order to provide an overall view of the effect of the two parameters.

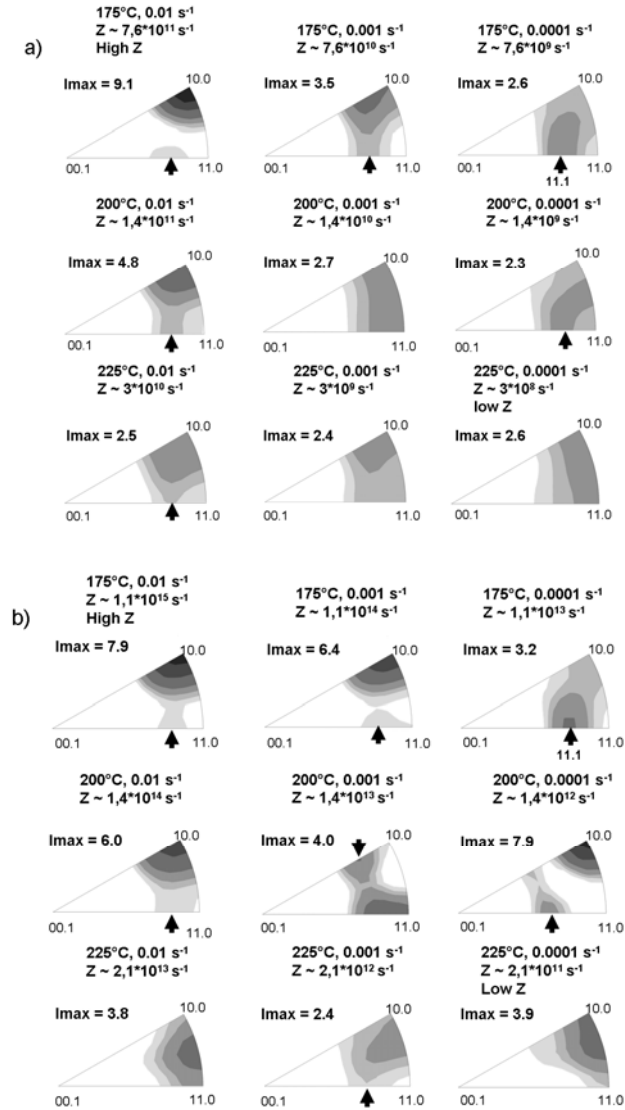


Fig. 8: Inverse pole figures of the fraction of the microstructure with a GOS of more than 2 ° for a) AZ31 and b) AZ61.

Two important aspects have to be considered in analysing the microstructure in this way. Firstly, the GOS constraint of 2 ° assumed is again chosen arbitrarily, but in this way only grains with relatively high orientation spread were taken into account. Secondly, it has to be emphasised that Fig. 8 displays the texture of that fraction of the original microstructure which remains unrecrystallised after undergoing deformation. It therefore does not represent the overall deformation texture of the material because parts of the microstructure analysed here underwent dynamic recrystallisation during deformation. Besides, the newly formed grains could also undergo deformation, thus

increasing their internal misorientation. Nevertheless, this analysis does enable some important aspects of the deformation texture to be revealed.

Fig. 8a shows the results for AZ31 with decreasing strain rate at the three temperatures used. In the case of the inverse pole figure obtained after testing at 175 °C and a strain rate of  $10^{-2} \text{ s}^{-1}$ , a strong  $\langle 10.0 \rangle$  fibre is found, which is related to the elongated grains shown in Fig. 4a. A low intensity is also found around the  $\langle 11.1 \rangle$  pole in this condition (see the arrow). With decreasing strain rate, the intensity at the  $\langle 11.1 \rangle$  pole increases and reaches a maximum at the lowest strain rate at 175 °C. At higher temperatures, its significance seems to be reduced. The same effects are found in AZ61 where even more testing conditions lead to strong  $\langle 10.0 \rangle$  components (Fig. 8b).

In summary, it can be concluded that such texture components also appear in the deformed state of grains despite the fact that the significance of the components are a complex function of achieved strain and the related fraction of unrecrystallised microstructure.

Al-Samman et al. [9] have shown in similar tests that a lower  $Z$  value promotes the thermal activation of non-basal slip modes such as  $\langle c+a \rangle$  pyramidal slip as well as enhancing DRX. During tensile testing in the extrusion direction, the distinct  $\langle 10.0 \rangle$  texture component persists and is understood to result from preferred deformation by prismatic  $\langle a \rangle$  slip. This texture component is accompanied by a second component,  $\langle 11.0 \rangle$  which is related to the  $\langle 10.0 \rangle$  pole by an angle of  $30^\circ$  and is associated with the recrystallised fraction of the microstructure or the result of double prismatic slip. It was furthermore noted that multiple slip systems will prevent the development of a single strong texture component and lead to the formation of a multi-component texture which can be very weak. It was also suggested that the thermal activation of

non-basal slip systems, e.g.  $\langle c+a \rangle$  slip leads to the formation of a texture component which is tilted away from the  $\langle 10.0 \rangle$  prismatic pole towards  $\langle 00.1 \rangle$ , e.g.  $\langle 10.1 \rangle$ . Although such components were not explicitly found in the present work, the broader intensity distribution observed along the arc between the  $\langle 10.0 \rangle$  and  $\langle 11.0 \rangle$  poles could hide such a kind of component. Furthermore, effects due to the ongoing deformation of the recrystallised fractions of the microstructure may also contribute to the pole figures presented in Fig. 8.

A correlation between the deformation mechanisms and DRX was made by Galiyev et al [26]. They reported that during plastic deformation of a ZK60 Mg alloy at temperatures lower than 200 °C, twinning and basal slip are the dominant mechanisms that accommodate the plastic strain. However, it was pointed out that this combination of deformation mechanisms can only insufficiently comply with the compatibility constraints at grain boundaries. Due to large elastic distortion at grain boundaries, the internal stresses could exceed the critical resolved shear stress (CRSS) for the activation of non-basal slip type  $\langle c+a \rangle$ , which at low temperatures is much higher than that for basal slip [27]. This is likely to increase the propensity to form recrystallisation nuclei. It was also reported that at intermediate temperatures (200-250 °C) the controlling mechanism of plastic deformation was the cross-slip of  $\langle a \rangle$  dislocations on non-basal planes. Such cross-slip was predominantly activated near the original grain boundaries where the stresses are highly concentrated and continuous absorption of dislocations in the low-angle boundaries results in a continuous dynamic recrystallisation mechanism; i.e., in the formation of new grains by rDRX. This could also occur during the deformation of the AZ31 and AZ61 alloys in this work.

Still, some aspects regarding the importance of deformation twins have to be highlighted. In this study, no evidence for deformation twinning was found, although the deformation was carried out at low temperatures around 200 °C. In case of extension twinning, this can be attributed to fine grained microstructure and the texture of the material [28, 29]. Such a texture is unfavourable for this twinning mode due to the preferential alignment of basal planes in the extrusion direction. Conversely, in both alloys the initial texture is suitable for the activation of contraction twinning since most of the grains have their c-axis perpendicular to the loading direction. It is also noteworthy, that there is evidence that this type of twins can be better activated if the temperature increases [30]. Contraction twins can change the texture due to reorientation and also serve as an effective site for recrystallisation due to their high stored energy, thus generating new grains with different orientations [31, 32]. However, the measurements in the context of this work did not reveal evidence of contraction twins especially not in the unrecrystallised fraction of the microstructure. It could be possible that contraction twins could serve as effective sites for initiating twin-induced recrystallisation, if they were present. Although no direct conclusion can be drawn about the importance of contraction twins as an active mechanism in this work, there is evidence that recrystallisation took place near the boundaries of the grains and this will be discussed more in detail in the following sections.

Contrary, the activation of non-basal  $\langle c+a \rangle$  slip and/or  $\langle a \rangle$  cross slip during tensile testing in this temperature range could influence the deformation texture and promote the formation of new recrystallised grains with a different orientation [26, 33].

#### 4.4 Texture of the recrystallised fraction of the microstructure

In order to separate details of the texture of the recrystallised fraction of the microstructure, IPFs of the fraction of the microstructure having a GOS < 1° are shown in Fig. 9. Two IPFs separate this fraction of the microstructure into smaller and larger grains where the average recrystallised grain size is used as a constraint. A similar analysis was applied in [16] in order to separate effects of the growth kinetics of grains with different orientations in Mg-Mn alloys containing rare earth elements.

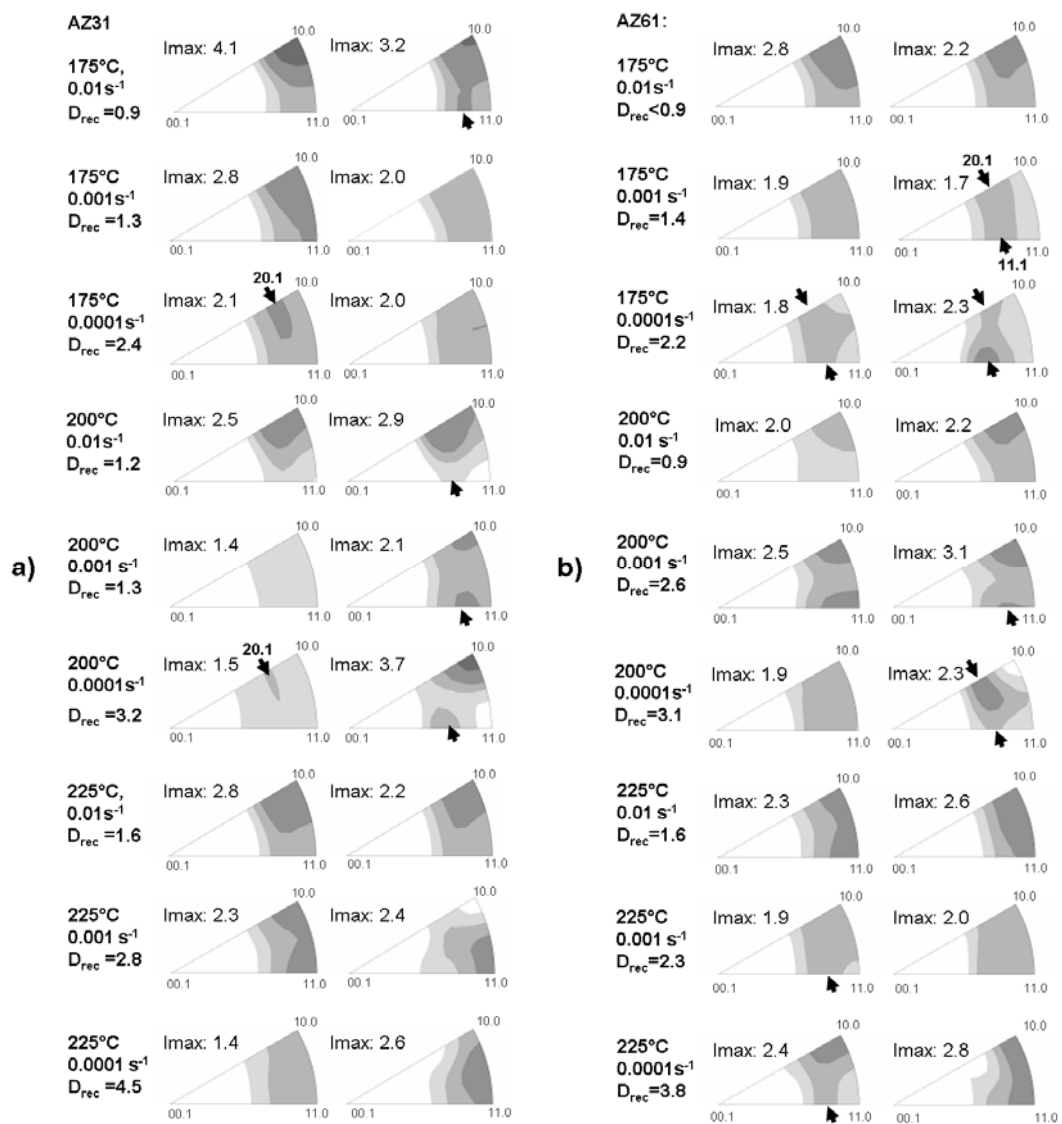


Fig. 9: Inverse pole figures of the fractions of the microstructure with a grain size smaller (left) and coarser (right) than the average recrystallised grain size for a) AZ31 and b) AZ61.

In AZ31, tested at 175 °C and  $10^{-2} \text{ s}^{-1}$  (high Z), the main texture component is the  $\langle 10.0 \rangle$  component which is visible in both the small and the coarse recrystallised grains, Fig. 9a. This component becomes less significant with decreasing strain rate. The same is found for AZ61, as shown in Fig. 9b. In AZ31, tested at 225 °C and  $10^{-4} \text{ s}^{-1}$  (low Z), a distinct  $\langle 11.0 \rangle$  texture component is observed which appears to be more pronounced in the large grains than in the small grains. However, this effect is not seen in the case of AZ61. Instead, the textures are very weak and sometimes the highest intensities are no longer located along the arc between the  $\langle 10.0 \rangle$  and  $\langle 11.0 \rangle$  poles, e.g. after testing at 225 °C and  $10^{-3} \text{ s}^{-1}$ . It is not possible to say if there is any preferential growth of grains with the resulting orientations along an arc between the  $\langle 20.1 \rangle$  and  $\langle 11.1 \rangle$  poles (see the arrows in different conditions for both alloys). It is again suggested that the significance of these intensities is a result of the lower intensities found along the arc between the  $\langle 10.0 \rangle$  and  $\langle 11.0 \rangle$  poles rather than the development of a distinct texture component. In the case of AZ31, there is also no significant growth effect of texture components other than the  $\langle 11.0 \rangle$  component at low Z. Unlike in the case of the above mentioned study [16], where preferential growth of a so-called “rare earth texture component” around the  $\langle 11.1 \rangle$  pole is found as a result of recrystallisation during an extrusion experiment, there is no preferential development of such a component in the case of the AZ31 and AZ61 samples in this study.

#### *4.5 Recrystallisation mechanisms*

The development of a texture with a  $\langle 11.0 \rangle$  component has been observed by various authors as a result of the growth of recrystallised grains in conventional Mg-Al-Zn alloys [8, 34]. It can be a result of DRX if fully recrystallised microstructures are

achieved [9, 35] or the result of static recrystallisation (SRX) [8]. The latter can be excluded as a possibility in this study, because samples were water-quenched immediately after testing. In the case of DRX, dDRX and rDRX have been reported to have different impacts on texture development. Both mechanisms lead to a necklace-type microstructure with fine recrystallised grains surrounding deformed, unrecrystallised grains. This type of microstructure is not seen in this study because most of the samples underwent very high strains and developed homogeneous microstructures as a result of DRX.

A close up of the microstructure of two samples deformed at  $175\text{ }^{\circ}\text{C}/10^{-2}\text{ s}^{-1}$  (Fig. 10a) and  $225\text{ }^{\circ}\text{C}/10^{-4}\text{ s}^{-1}$  (Fig. 10b) of AZ61 alloy allows the operative mechanisms of grain formation during recrystallisation to be investigated. Basically, the microstructural features of this alloy and the AZ31 alloy are quite comparable in both conditions, but AZ61 contains large particles, some of them larger than  $1\text{ }\mu\text{m}$ , which enables a consideration of their influence on the microstructure and the texture development. In this analysis, six grains were exemplarily investigated regarding their misorientation gradient. In both cases, lines of typical misorientation gradients of grains with the following characteristics were investigated and typical examples are shown: Line 1 shows the misorientation development in a deformed and unrecrystallised ( $\text{GOS} > 1^{\circ}$ ) grain whereas line 2 shows the same in a recrystallised grain ( $\text{GOS} < 1^{\circ}$ ), both grains are in the vicinity of a second phase particle (coloured in black). The other lines show the respective development in grains which are not near particles. Line 3 shows a development of the misorientation from a deformed grain into a new or developing recrystallised grain. Finally, line 4 shows the misorientation development over three recrystallised grains ( $\text{GOS} < 1^{\circ}$ ) in the vicinity of a deformed grain ( $\text{GOS} > 1^{\circ}$ ).

In Fig. 10a after testing at high  $Z$ , lines 1 and 2 show a progressive increase of misorientation from the grain centre to the particle in close vicinity. This is not surprising for the deformed grain, but in case of the recrystallised grain such a finding could be indicative for PSN being operative [36].

For the test at low  $Z$  in Fig. 10b this is not found. Although line 1 also reveals a continuous increase of the misorientation, line 2 shows a misorientation profile close to zero along the measured distance. In this case a similar finding is shown for line 3 and the misorientation shown in line 4 over three adjacent recrystallised grains confirms a low misorientation gradient in the respective grains. This finding is consistent with a dDRX mechanism as a source of these newly developed grains. Unlike this, in Fig. 10a at high  $Z$ , the two latter lines exhibit a notable increase in the misorientation even in the recrystallised grains. This finding is consistent with a rDRX mechanism. It is noteworthy, that there is no significant difference between the recrystallised grains in the vicinity of particles to those developing around coarse deformed grains. Consequently, this evidence leaves the interpretation with a PSN mechanism as a controlling mechanism to produce important changes in microstructure and texture in doubt. Indeed, this finding confirms the affirmation of Robson et al. [36] that PSN is in competition with new grains formed at other sites. Then, this mechanism most likely did not take control on the microstructure and therefore on the texture development.

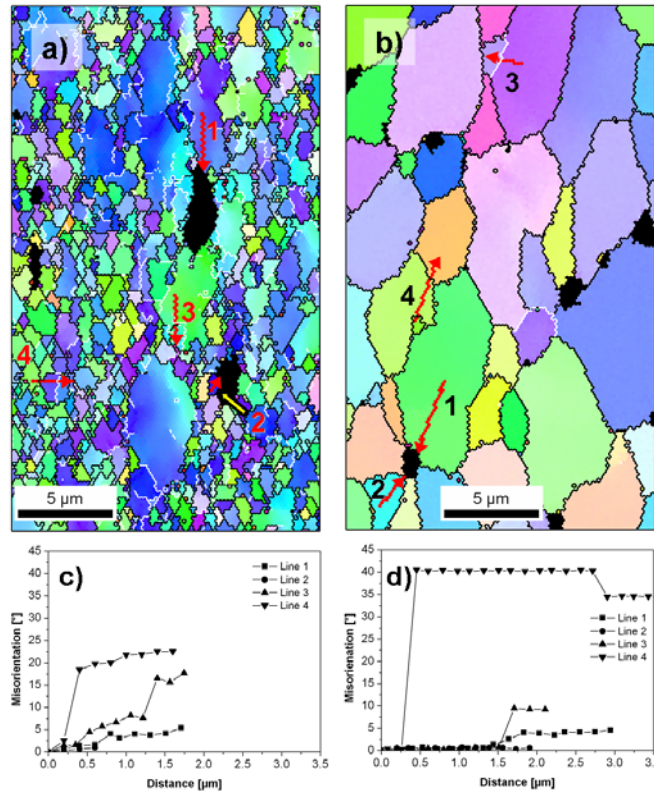


Fig. 10: Orientation map of AZ61 samples at a)  $175\text{ }^{\circ}\text{C}/10^{-2}\text{ s}^{-1}$  and b)  $225\text{ }^{\circ}\text{C}/10^{-4}\text{ s}^{-1}$ , and misorientation profiles of selected grains c)  $175\text{ }^{\circ}\text{C}/10^{-2}\text{ s}^{-1}$  and d)  $225\text{ }^{\circ}\text{C}/10^{-4}\text{ s}^{-1}$ ; Line 1 (unrecrystallised grain) and line 2 (recrystallised grain) are in the vicinity of a particle whereas line 3 is along a developing small angle grain boundary and line 4 shows the grain boundary misorientation of 3 recrystallised grains (high angle grain boundaries coloured in black, low angle grain boundaries coloured in white).

Thus, it is hypothesised that basically two different DRX mechanisms contribute differently to the texture development of the recrystallised fraction of the microstructure as a function of  $Z$ . At low  $Z$ , where the  $\langle 11.0 \rangle$  texture component is found preferentially in larger grains with low GOS, i.e. larger recrystallised grains, it can be anticipated that dDRX determines the microstructural development whereas at higher  $Z$  this is not the case. At high  $Z$  the microstructural development appears to be limited with respect to recrystallisation, i.e. partly recrystallised microstructures result.

#### *4.6 Grain boundary sliding and dynamic precipitation*

Another important deformation mechanism that has to be considered as a texture contributing mechanism is grain boundary sliding (GBS). In earlier work, it was demonstrated that GBS was an operative mechanism responsible for the large tensile elongation reached in the case of the AZ61 alloy [20]. It has been pointed out [37, 38] that textures can be strongly affected when GBS takes place during deformation. It is agreed that GBS progressively weakens the texture and that, at large strains, the texture is more random e.g. as a result of superplastic deformation [39]. Then it can be assumed that a potential texture change due to GBS is most significant at intermediate  $Z$  in AZ61 alloy where the highest elongations to failure were achieved and the highest fraction of the microstructure could be affected.

It is also widely accepted that GBS can be enhanced if a stable microstructure with small and equiaxed grains is maintained during deformation [40]. A common technique for restricting dynamic grain growth during deformation at high temperatures is to use a dispersion of fine particles [41]. Taking into account the equiaxed microstructures and very fine grain sizes according to Figs. 4 and 5, a close inspection of precipitates was carried out and the results are presented in Fig. 11.

Interestingly, dynamic precipitation took place during deformation of the AZ31 alloy at 175 °C at all strain rates (Fig. 11a). At this temperature, fine and homogeneously distributed precipitates are mainly located along grain boundaries. As the temperature rises to 200 and 225 °C, the amount of precipitates decreases. The same is found in the AZ61 alloy in which coarser precipitates than in the AZ31 alloy are found (Fig. 11b). EDS analysis revealed two types of precipitates in both alloys. The first is the Mg-Al type ( $Mg_{17}Al_{12}$ ) located mainly on grain boundaries and the second is the Al-Mn type ( $Al_8Mn_5$ ) located within the grains. It should be noted that the Al-Mn

particles were present in “stringers” parallel to the extrusion direction after extrusion in both alloys. During tensile testing, they only became fragmented.

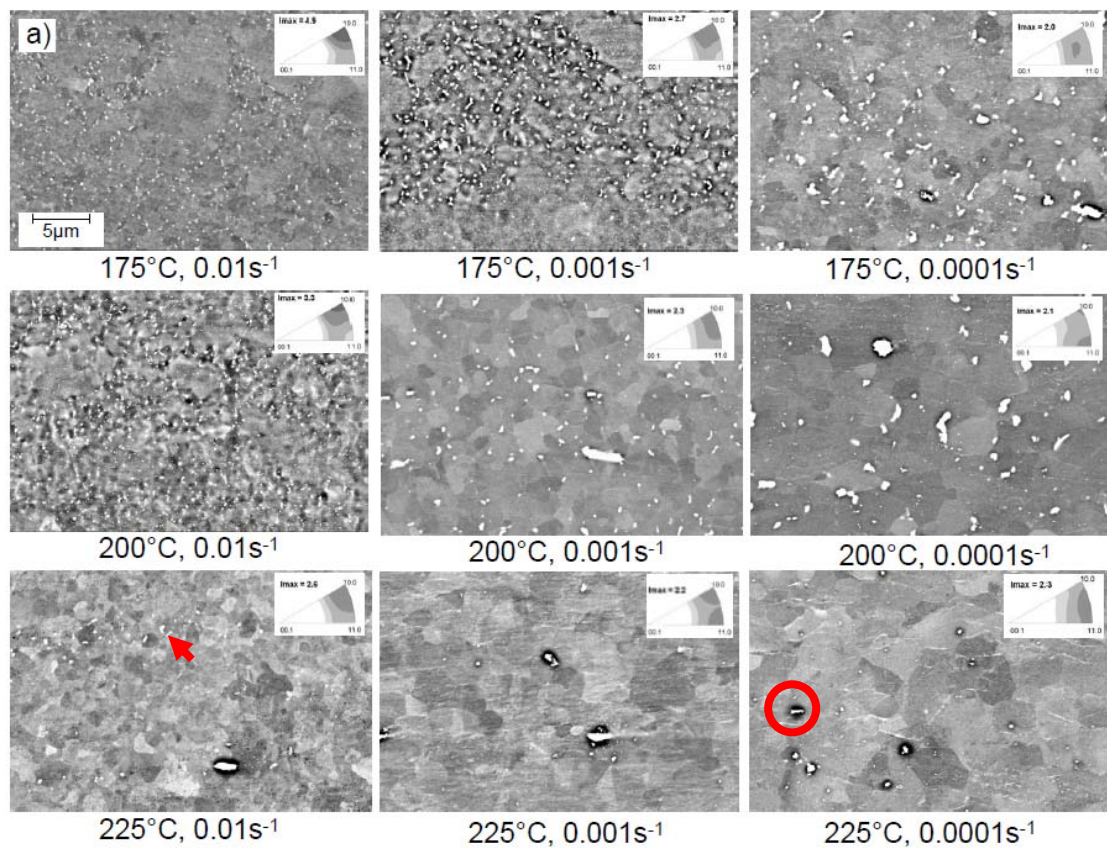
The  $\text{Mg}_{17}\text{Al}_{12}$  particles appear in the AZ31 alloy at 175 and 200 °C with only few being found at 225 °C/ $10^{-2} \text{ s}^{-1}$  (see the arrow in Fig 11a). At 225 °C/ $10^{-4} \text{ s}^{-1}$  only  $\text{Al}_8\text{Mn}_5$  particles are present (inside the circle). The AZ61 alloy exhibits  $\text{Mg}_{17}\text{Al}_{12}$  particles even after testing at 225 °C/ $10^{-4} \text{ s}^{-1}$ , but they are coarse and not finely distributed. It was demonstrated in an earlier work [20], that such a particle coarsening and related void formation leads to a decrease of the elongation to failure if  $Z$  was decreased compared to the high elongations at intermediate  $Z$  in the case of this alloy.

It is well known that second-phase particles, particularly if homogeneously and finely distributed and small ( $\leq 1 \mu\text{m}$ ), can exert significant pinning on grain boundaries [19]. This particle pinning effect can restrict the mobility of grain boundaries and may therefore also have an influence on grain growth.

For the alloy AZ31, Yi et al [8] demonstrated that recrystallised grains generated during an extrusion experiment were mainly produced by rDRX and that the high degree of internal misorientation (stored energy) of these grains provides the driving force for the grains to grow during annealing treatments. Furthermore, grain growth plays an important role in changing the texture of the profile. Such grain growth changed the texture distribution from the  $\langle 10.0 \rangle$  pole to the  $\langle 11.0 \rangle$  pole.

In the present case, a possible restriction of grain growth could be directly related to the amount, size and distribution of the secondary particles ( $\text{Mg}_{17}\text{Al}_{12}$ ) produced by dynamic precipitation that could be another reason why during tensile deformation the significance of the intensities of the  $\langle 10.0 \rangle$  and  $\langle 11.0 \rangle$  poles are highly reduced, i.e. at 175 °C fine and well distributed precipitates of the  $\text{Mg}_{17}\text{Al}_{12}$  phase are located along

grain boundaries and a high intensity around the  $\langle 11.1 \rangle$  pole is observed rather than around the  $\langle 11.0 \rangle$  pole. Indeed, at this temperature the  $\langle 11.1 \rangle$  pole intensity reaches the maximum at the lowest strain rate for both alloys (see the IPF insets in Fig. 11). As the temperature increases, the  $\text{Mg}_{17}\text{Al}_{12}$  phase dissolves in the case of the AZ31 alloy, whereas in the AZ61 alloy coalescence of coarse precipitates takes place and they are no longer homogeneously distributed. This could reduce the effectiveness of the particle pinning effect, and as a result, the typical texture with higher intensities along the arc between the  $\langle 10.0 \rangle$  and  $\langle 11.0 \rangle$  developed, e.g. after testing at  $225\text{ }^\circ\text{C}/10^{-4}\text{ s}^{-1}$  (low Z). Vice versa, it is hypothesised that small particles along grain boundaries restrict the formation of the distinct  $\langle 11.0 \rangle$  texture rather than being responsible for the development  $\langle 11.1 \rangle$  texture component.



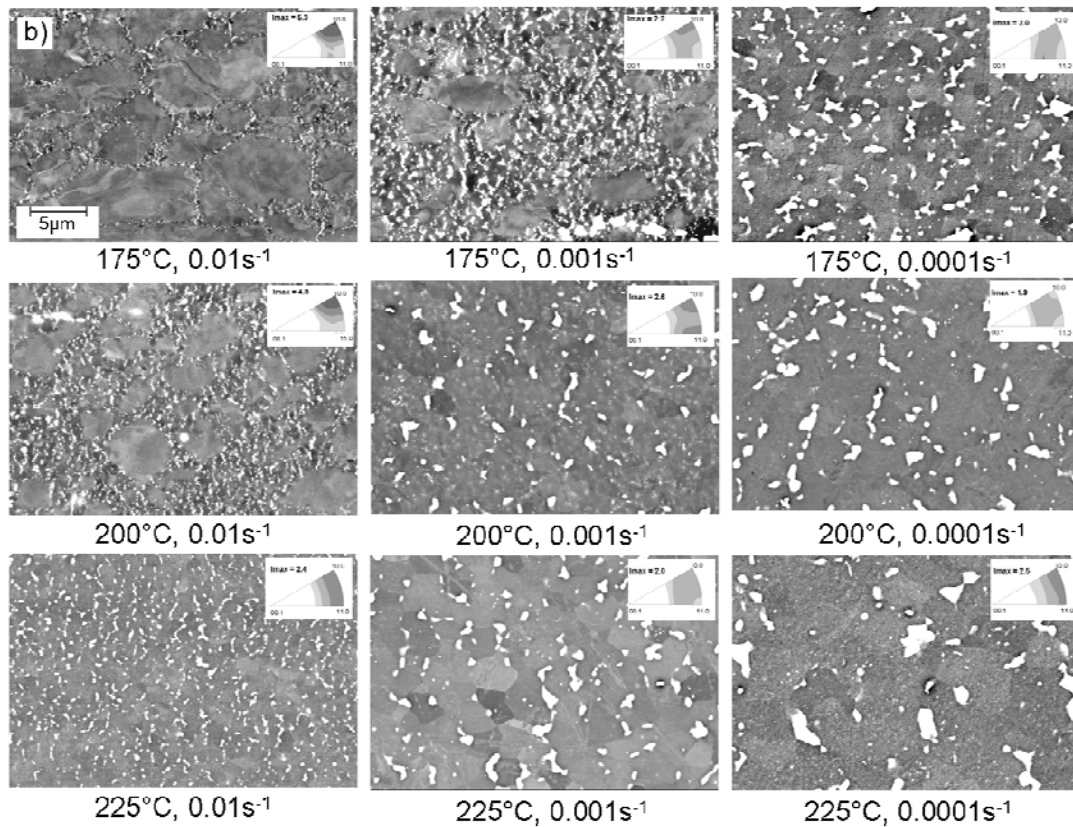


Fig. 11: Micrographs after deformation showing precipitation effects in  
a) AZ31 and b) AZ61

Grain growth restricting mechanisms have received some attention in recent works where they were investigated in the context of RE additions to Mg alloys [11,16]. It was shown that RE additions to Mg alloys affect the microstructure by restricting grain growth due to solute segregations or particle pinning [11, 42]. In addition to this, textures that show similarities to the ones observed in this investigation are found, specifically the development of a  $\langle 11.1 \rangle$  texture component [14, 16, 17].

As described in [16], the RE component is strongly influenced by the different degrees of recrystallisation obtained, which depend on the specific RE used. Alloys containing RE elements exhibit weaker textures compared to alloys without RE elements. Moreover, it was pointed out that the texture component depends on the size of the recrystallised grains. Once the microstructure is determined by a RE

texture, larger recrystallised grains exhibit a distinct  $\langle 11.1 \rangle$  component whereas smaller recrystallised grains have the original  $\langle 10.0 \rangle$  component.

It was noted by Stanford et al [14] that the  $\langle 11.1 \rangle$  texture component was only present for certain extrusion conditions, i.e. a low extrusion temperature, therefore increasing  $Z$ .

Although a similar behaviour regarding the texture development is found in this work, the direct comparison of larger and smaller recrystallised grains does not reveal clear evidence for a preferential development of such a texture component in larger grains (Fig. 9). Therefore, besides the fact that grain growth restriction is likely to be enhanced in those samples tested at higher  $Z$ , the resulting effect on the texture of the samples is obviously not the development of a specifically new texture component like found in RE containing Mg alloys.

### **Summary and conclusions**

Fine-grained hydrostatically extruded round bars of the alloys AZ31 and AZ61 were used for tensile tests in the extrusion direction at different temperatures and strain rates. Flow curve analysis of the influence of such parameters was based on one parameter, the temperature compensated strain rate  $Z$ . The flow behaviour of the materials was associated with microstructural changes due to dynamic recrystallisation, grain growth, grain boundary sliding and dynamic precipitation. The mechanisms that take control on the microstructure development vary with the testing parameters applied.

The findings in the microstructures after testing favour dDRX as a grain formation mechanism if  $Z$  was low whereas rDRX corresponds to the findings if  $Z$  was high. Although PSN as another grain nucleation mechanism cannot be excluded, it is

unlikely that this mechanism takes a specific role in the overall texture development. dDRX was associated with the formation of a typical  $\langle 11.0 \rangle$  texture component at low  $Z$  and with increasing  $Z$  this texture component did not appear significantly any more.

GBS is also likely to contribute to weak textures especially in those samples that reached high elongations to failure. Especially in the case of AZ61 this leads to peak elongations at intermediate  $Z$  and concurrent changes in the texture development.

Furthermore, precipitates, that are small and concentrated along grain boundaries in some cases, are prone to influence the growth of recrystallised grains so that growth restrictions can result for grains that would develop a conventional  $\langle 11.0 \rangle$  orientation.

### **Acknowledgments**

The authors would like to thank Dr. P.A. Beaven at the Helmholtz-Zentrum Geesthacht for his comments and discussion. JVH is grateful with CONACyT Mexico for the financial support for the stay in Germany and with the technician staff of the WZW group at Helmholtz Zentrum Geesthacht in Germany for sample preparation.

### **References**

- [1] Dillamore IL, Roberts WT, Metall Rev 1965;10:271.
- [2] Bohlen J, Yi SB, Swiostek J, Letzig D, Brokmeier HG, Kainer KU. Scripta Mater 2005;53:259–264.
- [3] Partridge PG. Metall Rev 1967;12:169-194.
- [4] Christian JW, Mahajan S. Prog Mater Sci 1995;39:1-157.
- [5] Dudamell NV, Ulacia I, Gálvez F, Yi S, Bohlen J, Letzig D, Hurtado I, Pérez-Prado MT. Acta Mater 2011;59:6949-6962.
- [6] Sandlöbes S, Zaefferer S, Schestakow I, Yi S, Gonzalez-Martinez R. Acta Mater 2011;59:429–439
- [7] Barnett MR, Sullivan A, Stanford N, Ross N, Beer A. Scripta Mater 2010;63:721-724.
- [8] Yi S, Brokmeier HG, Letzig D. J. Alloys Comp 2010;506:364–371.
- [9] Al-Samman T, Li X, Ghosh Chowdhury S. Mater Sci Eng 2010;A527:3450-3463.
- [10] Wang M, Xin R, Wang B, Liu Q. Mater Sci Eng 2011;A528:2941–2951.
- [11] Hadorn JP, Hantzsche K, Yi S, Bohlen J, Letzig D, Wollmershauser JA, Agnew SR. Metall Mater Trans 2012;A43:1347-1362.
- [12] Bohlen J, Nürnberg MR, Senn JW, Letzig D, Agnew SR. Acta Mater 2007;55:2101–2112.
- [13] Wendt J, Hantzsche K, Bohlen J, Kainer KU, Yi S, Letzig D. In: Kainer KU, editor. Magnesium, 8th International Conference on Magnesium Alloys and their Applications. Weinheim: VCH Wiley; 2010. p. 551 – 556.

- [14] Stanford N, Barnett MR. *Mater Sci Eng* 2008;A496:399-408.
- [15] Stanford N, Atwell D, Beer A, Davies C, Barnett MR. *Scripta Mater* 2008;59:772–775.
- [16] Bohlen J, Yi S, Letzig D, Kainer KU. *Mater Sci Eng* 2010;A527:7092-7098.
- [17] Stanford N, Atwell D, Barnett MR. *Acta Mater* 2010;58:6773-6783.
- [18] Ball EA, Prangnell PB. *Scripta Mater* 1994;31:111-116.
- [19] Humphreys FJ, Hatherly M. *Recrystallization and related annealing phenomena*. Oxford: Elsevier; 2004. p. 285, 310, 392
- [20] Victoria-Hernández J, Hernández-Silva D, Yi SB, Letzig D, Bohlen J. *Mater Sci Eng* 2011;A530:411–417.
- [21] Swiostek J, Göken J, Letzig D, Kainer KU. *Mater Sci Eng* 2006;A424:223-229.
- [22] Sellars CM. *Mater Sci Tech* 1990;6:1072–1081.
- [23] McQueen HJ, Ryan ND. *Mater Sci Eng* 2002;A322:43–63.
- [24] Zener C, Hollomon JH. *J. Appl. Phys.* 15 (1994) 22.
- [25] Liu J, Cui Z, Li C. *Comput Mater Sci* 2008;41:375–382.
- [26] Galiyev A, Kaibyshev R, Gottstein G. *Acta Mater* 2001;49:1199-1207.
- [27] Ion SE, Humphreys FJ, White SH. *Acta Metall* 1982;30:1909.
- [28] Zhang Z, Wang M, Li Z, Jiang N, Hao S, Gong J, Hu H. *J. Alloys Comp* 2011;509:5571-5580.
- [29] Dobron P, Chmelik F, Yi SB, Parfenenko K, Letzig D, Bohlen J. *Scripta Mater* 2011;65:424-427.
- [30] Yoshinaga H, Obara T, Morozumi S. *Mater Sci Eng* 1973;12:255-264.
- [31] Barnett MR. *Mater. Sci. Eng.* 2007;A464:8-16.
- [32] Kim HL, Lee JH, Lee CS, Bang W, Ahn SH, Chang YW. *Mater Sci Eng* 2012;A558:431-438.
- [33] Yi S, Bohlen J, Heinemann F, Letzig D. *Acta Mater* 2010;58:592-605.
- [34] Lorimer GW, Mackenzie LWF, Humphreys FJ, Wilks T. *Mater Sci Forum* 2004;467 – 470:477 – 482.
- [35] Bohlen J, Swiostek J, Brokmeier HG, Letzig D, Kainer KU. In: Luo AA, Neelameggham NR, Beals RS, editors. *Magnesium Technology*, San Antonio: TMS;2006. p. 213-217.
- [36] Robson JD, Henry DT, Davis B. *Acta Mater* 2009;57:2739–2747.
- [37] Kim WJ, Chung SW, Chung CS, Kum D. *Acta Mater* 2001;49:3337-3345
- [38] Watanabe H, Fukusumi M. *Mater Sci Eng* 2008;A477:153–161.
- [39] Del Valle JA, Ruano OA. *Acta Mater* 2007;55:455–466.
- [40] Nieh TG, Wadsworth J, Sherby OD. *Superplasticity in metals and ceramics*. Cambridge University Press; 1997. p. 22-23
- [41] Bate P. *Acta Mater* 2001;49:1453-1461.
- [42] Hadorn JP, Hantzsche K, Yi S, Bohlen J, Letzig D, Agnew SR. *Metall Mater Trans* 2012;A43:1363-1375